# Effect of Surface Immobilization on Intramolecular and Intermolecular Electron Transfer in a Chromophore−Donor−Acceptor Assembly

**Milan Sykora, John C. Yang, and Thomas J. Meyer***

*Department of Chemistry, University of North Carolina at Chapel Hill, Chapel Hill, North Carolina 27599-3290, and Los Alamos National Laboratory, MS A127 ADSR, Los Alamos, New Mexico 87545*

*Received: March 31, 2004; In Final Form: September 8, 2004*

A chromophore−donor−acceptor assembly $[Ru(bpyCOOH)(bpyCH_2MV^{2+})(bpyCH_2PTZ)]^{4+}$ **(1)** (where bpyCOOH = 4-carboxylic acid-4′-methyl-2,2′-bipyridine, $bpyCH_2MV^{2+}$ = 1-[(4′-methyl-2,2′-bipyridin-4-yl)methyl]-1′-methyl-4,4′-bipyridinediium, and $bpyCH_2PTZ$ = 10-[(4′-methyl-2,2′-bipyridin-4-yl)methyl]-phenothiazine) has been adsorbed on the surface of nanocrystalline $ZrO_2$ and its excited state properties studied by emission and transient absorption spectroscopy. In deaerated acetonitrile solution, the complex emits weakly with an emission quantum yield of $\phi_{em} \approx 0.01$ with an excited-state lifetime of $\tau \approx 20$ ps. Emission from the surface-adsorbed complex is intense, with $\phi_{em} \approx 0.4$ and $\tau \approx 40$ ns. The increase in emission on the surface is likely due to a significant inhibition to the electron-transfer quenching of the metal-to-ligand charge transfer (MLCT) excited state caused by surface adsorption-induced changes in the redox potentials. Transient (nanosecond time scale) absorption monitoring, following laser flash photolysis, reveals the presence of a transient or transients that are formed during the flash. Transient spectral changes that occur during and after the flash are consistent with the formation and decay of the intermediate $ZrO_2-[Ru(bpyCOOH)(bpyCH_2MV^{+\bullet})(bpyCH_2PTZ^{+\bullet})]^{4+}$. It returns to the ground state by both intramolecular and intermolecular processes. Intramolecular electron transfer occurs with $k_{BET} = 6.3 \times 10^6\ s^{-1}$ ($\tau = 160$ ns), which is comparable to the rate constant for back-electron transfer in solution. The back-electron transfer is a second-order process and is much slower, with $k_{BET} = 390\ M^{-1}\ s^{-1}$ ($\tau = 2.6$ ms).

## Introduction

Photochemical electron transfer in fluid solution is a well-studied phenomenon, and transition-metal complexes of Ru(II), Os(II), and Re(I) have had an important role, because of their desirable photophysical and electron-transfer properties. One of the reasons for interest is possible applications in artificial photosynthesis and molecular-level devices.[1−5] Practical devices demand the incorporation of photochemically and redox-active components in rigid matrixes or their immobilization on surfaces,[4,6−16] and this can cause significant changes in excited-state properties and electron-transfer behavior.[17−19]

We recently reported on the preparation and characterization of the chromophore−donor−acceptor assembly $[Ru(bpyCOOH)(bpyCH_2MV^{2+})(bpyCH_2PTZ)]^{4+}$ **(1)**, which is shown below.[20]

Following visible laser flash excitation in deaerated acetonitrile at room temperature (RT), this assembly undergoes a sequence of rapid intramolecular electron-transfer events to form a $MV^{+\bullet}/PTZ^{+\bullet}$ redox-separated state with an efficiency of $\Phi_{RSS} = 0.35$. After the assembly has been formed, it undergoes $MV^{+\bullet} \rightarrow PTZ^{+\bullet}$ back-electron transfer, giving the ground state with $k_{BET} = 6.3 \times 10^6\ s^{-1}$.[20] When incorporated as a minor component into a derivatized polystyrene assembly with a majority of $[Ru(bpyCOOH)(bpy)_2]^{2+}$ (where bpyCOOH is 4-(COOH)-4′-Me-2,3′-bipyridine) sites appended as "antennae", sequential excitation, energy migration, and sensitization of electron transfer in **1** mimics the photosynthetic reaction center.[21]

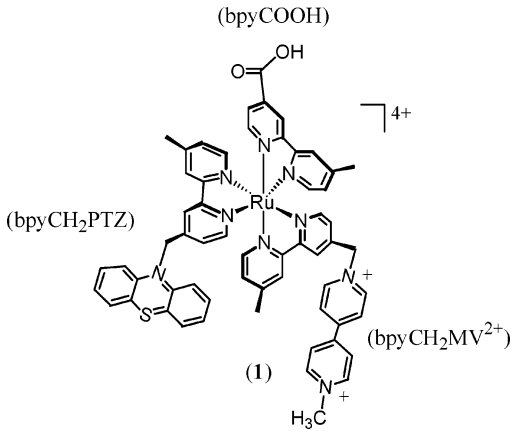


In the present work, we have investigated the properties of **1** adsorbed on the surface of nanocrystalline $ZrO_2$ and found evidence for relatively unperturbed $MV^{+\bullet} \rightarrow PTZ^{+\bullet}$ intramolecular back-electron transfer, as well as a much slower component arising from $MV^{+\bullet} \rightarrow PTZ^{+\bullet}$ intermolecular electron transfer between spatially separated adsorbed molecules on the surface.

## Experimental Section

Complex **1** was available as its $PF_6^-$ salt from previous studies.[20,21] The preparation of the complex has been described previously.[20]

Thin films of nanocrystalline $ZrO_2$ deposited on a glass substrate were prepared by the sol−gel method, following a

* Author to whom correspondence should be addressed. E-mail: tjmeyer@lanl.gov.

10.1021/jp040260t CCC: $30.25 © 2005 American Chemical Society
Published on Web 01/11/2005

modified literature procedure.[22] This procedure yields almost optically transparent, ~5-$\mu$m-thick mesoporous films consisting of interconnected ~20-nm $ZrO_2$ particles. The $ZrO_2$ films were modified by surface adsorption of the complex by immersing the film into a $10^{-4}$ M $CH_3CN$ solution of **1**. The absorption spectrum of **1** is unchanged upon immobilization on the nanocrystalline surface and was used for the determination of surface coverage.

Ultraviolet−visible (UV−vis) measurements were made with a Hewlett−Packard model HP-8452 diode array spectrometer and referenced against a solvent blank (ethanol, EtOH). The $ZrO_2$ electrodes were placed in a 1-cm cuvette that contained EtOH and were positioned against the side of the cell for each measurement. After the subtraction of a spectrum of a $ZrO_2$ blank film, the number of moles of metal complex per square centimeter of projected surface area of the nanocrystalline film ($\Gamma_{pro}$(mol/cm$^2$)) was calculated from the relationship $A(\lambda) = \Gamma_{pro}\sigma(\lambda)$, where $A(\lambda)$ is the absorbance of the film and $\sigma(\lambda)$ is the absorption cross section (in units of cm$^2$/mol) obtained from the decadic molar extinction coefficient ($\epsilon$, given in terms of $M^{-1}$ $cm^{-1}$) by multiplication by 1000 cm$^3$/L. In the analyses, $\epsilon$(458 nm) = 13 000 $M^{-1}$ $cm^{-1}$ were used for adsorbed **1**. A monolayer surface coverage of ~$6.5 \times 10^{-11}$ mol/cm$^2$ for **1** can be calculated if spheres with radii of 9 Å (estimated using van der Waals radii) are assumed to be closely packed on a flat surface (neglecting the counterions). The actual coverage ($\Gamma$) is given by $\Gamma = \Gamma_{pro}/\eta$, where $\eta$ is a surface roughness factor, which is defined as the ratio of the effective surface area of the nanocrystalline films to its projected area. It can be calculated by dividing $\Gamma_{pro}$ for a fully loaded surface by $6.5 \times 10^{-11}$ mol/cm$^2$. The surface was assumed to be fully loaded, following the exposure of the film to a $10^{-4}$ M $CH_3CN$ solution of **1** overnight. For films 4−6 $\mu$m thick, surface roughness factors of 500−700 (500−700 effective monolayers) were calculated, which is consistent with a multilayer structure of interconnected $ZrO_2$ particles.

Measurements of the excited-state lifetime and transient absorbance were performed using a Surelite II-10 (Continuum) Nd:YAG−OPO laser as an excitation source on acetonitrile exposed and dry samples. The excitation wavelength was 464 nm, and the power of the beam (defocused to ~3 cm$^2$) at the sample was 1.2 mJ/pulse-cm$^2$. The pulse width was 5−7 ns (full width at half maximum, fwhm). The excitation beam from the laser irradiated the sample (at a 45° angle) perpendicular to the optical axis of an Applied Photophysics laser kinetic spectrometer that consisted of a 150-W pulsed xenon lamp, a f3.4 monochromator, and a photomultiplier tube (PMT) (Hammamatsu model R446). The output from the PMT was coupled to a LeCroy model 7200A oscilloscope that had been interfaced with an IBM personal computer (PC). Electronic synchronization and control of the experiment was achieved using electronics of local design. Kinetic traces (average of 1000) decaying to >5 lifetimes of the transient observed were acquired and averaged at each wavelength. The average decay curves were fit to an appropriate kinetic model, using SigmaPlot (Jandel Scientific, Inc.). The decay kinetics observed from air-exposed dry $ZrO_2$−[Ru(bpyCOOH)(bpyCH$_2$MV$^{2+}$)(bpyCH$_2$PTZ)](PF$_6$)$_4$ films in aerated or argon-dearated acetonitrile exposed films were virtually identical.

Transient absorbance kinetic traces for an acetonitrile solution of **1** and kinetic traces for the emission decay of surface-adsorbed **1** were fit to the expression in eq 1:

$$I(t) = a\exp(-kt) \tag{1}$$

with $k = 1/\tau$. (The data were also fit to two- and three-exponential expressions. While these resulted in qualitatively better fits, the calculated average lifetimes coincided with the lifetime obtained by fitting the data to eq 1.)

There were both long and short components in the transient absorbance traces for surface-adsorbed **1**. The decay data were first fit to the second-order, equal-concentration expression in eq 2, to extract kinetic parameters for the long-lived component.

$$I(t) = I(t_0)\left(\frac{1}{k't+1}\right) \tag{2}$$

This contribution to the total absorbance−time ($A-t$) trace was numerically subtracted from the remaining signal, using the parameters $I(t_0)$ and $k'$ that were extracted from kinetic fits. The resulting differential trace was then fit to eq 1 to extract kinetic parameters for the short-lived component. The average lifetimes extracted from the differential trace and the transient absorbance lifetime of **1** in solution were, coincidentally, almost identical with the value $\tau \approx 160$ ns.

Cyclic voltammetric experiments were conducted with a model PAR 273 potentiostat, using a standard three-electrode configuration in a three-compartment cell in 0.1 M [*n*-N(C$_4$H$_9$)$_4$]-PF$_6$ in $CH_3CN$. The reference electrode was Ag/AgNO$_3$ (0.1 M TBAH and 0.01 M AgNO$_3$ in $CH_3CN$), which was 300 mV more positive than SCE, as measured by the ferrocene$^{+/0}$ couple at 0.40 V vs SCE. The counter electrode was platinum, and the working electrode was the derivatized $ZrO_2$ electrode.

## Results and Discussion

**Electron-Transfer Quenching.** In acetonitrile solution, $Ru^{II} \rightarrow$ bpy metal-to-ligand charge-transfer (MLCT) excitation is followed by electron transfer to the appended $MV^{2+}$ group on the time scale of tens of picoseconds.[23,24] This sequence results in the redox-separated (RS) state, shown in eq 3.

$$\begin{array}{l}[Ru^{III}(bpy^{-\bullet}COOH)(bpyCH_2MV^{2+})(bpyCH_2PTZ)]^{4+*} \\ \quad\uparrow h\nu \qquad\qquad [Ru^{II}(bpyCOOH)(bpyCH_2MV^{+\bullet})(bpyCH_2PTZ^{+\bullet})]^{4+*} \\ [Ru^{II}(bpyCOOH)(bpyCH_2MV^{2+})(bpyCH_2PTZ)]^{4+} \quad k_{BET}\end{array} \tag{3}$$

As suggested in eq 3, there is an asymmetry in the bpy acceptor ligands with the bpyCOOH ligand (or the surface ester form, bpyC(O)O−Zr ≡) being the lowest-energy acceptor, based on substituent effects.

Back-electron transfer, which is described with $k_{BET}$ in eq 3, is significantly slower ($k_{BET} = 6.3 \times 10^6$ $s^{-1}$), because it lies in the inverted region and occurs with a Gibbs free energy change of $\Delta G° \approx -1.15$ eV.

Adsorption of the complex on the surface of $ZrO_2$ nanoparticles has a pronounced effect on the dynamics of intramolecular electron-transfer quenching, as shown by lifetime and relative emission quantum yield measurements (Table 1). In contrast to the very weak emission (lifetime of $\tau \approx 20$ ps , $k \approx 6 \times 10^{10}$ $s^{-1}$) in acetonitrile,[20,23,24] there is a resolvable emission on $ZrO_2$ (Figure 1). Kinetic analysis of the emission decay, using the expression in eq 1, yields a lifetime of ~40 ns ($k \approx 2.5 \times 10^7$ $s^{-1}$).

The comparison between solution and surface lifetimes shows that there is a significant inhibition to electron-transfer quenching of the MLCT excited state on the surface with the rate constant for quenching decreasing from $k_q \approx 6 \times 10^{10}$ $s^{-1}$ (see refs 23 and 24) to $\langle k_q \rangle = 2.5 \times 10^7$ $s^{-1}$. This is not a microheterogeneity effect, with only a fraction of the sites on the nanocrystalline surface undergoing rapid quenching. If this were the case, there

**TABLE 1: Electrochemical and Photophysical Data**

| complex | $E_{1/2}$ values (V, vs SSCE)[a] $Ru^{III/II}$ | $PTZ^{+/0}$ | $MV^{2+/+}$ | emission maxima, $\lambda_{em}$(max) (nm)[b] | emission yield, $\Phi_{em}$ ($\times 10^2$)[b,c] | lifetime, $\tau$ (ns)[b] | $k_q$ ($\times 10^7$ $s^{-1}$) |
|---|---|---|---|---|---|---|---|
| $[Ru(bpyCOOH)(bpyCH_2MV^{2+})(bpyCH_2PTZ)]^{4+}$ | 1.31 | 0.81 | −0.34 | 672 | ~0.01 | 0.02 | 6000 |
| $ZrO_2$-$[Ru(bpyCOOH)(bpyCH_2MV^{2+})(bpyCH_2PTZ)](PF_6)_4$[d] | 1.41 | 0.94 | | 672 | 0.4 | 40 | 2.5 |

[a] $E_{1/2}$ values from cyclic voltammetry measurements in $CH_3CN$, 0.1 M TBAH at room temperature. Currents for the $MV^{2+/+}$ couple were too low to determine $E_{1/2}$ accurately. This is presumably due to slow kinetics of $MV^+ \rightarrow MV^{2+}$ charge hopping across the $ZrO_2$ surface. [b] In argon-deaerated $CH_3CN$ at room temperature. [c] Emission efficiency measured versus a $[Ru^{II}(bpy)_3](PF_6)_2$ ($\phi_{em} = 0.062$) standard. [d] The data reported are for films with 100% fractional surface coverage by the complex ($\Gamma \approx 6.5 \times 10^{-11}$ mol/cm$^2$). The actual formulation of the surface may be $ZrO_2$−$[O_2CbpyRu(bpyCH_2MV^{2+})(bpyCH_2PTZ)](PF_6)_3$, as noted in the text.

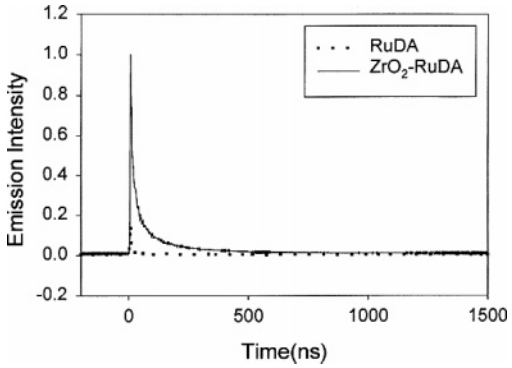


**Figure 1.** Time-resolved emission decay trace for $[Ru(bpyCOOH)(bpyCH_2MV^{2+})(bpyCH_2PTZ)]^{4+}$ (RuDA, dotted line) and $ZrO_2$−$[Ru(bpyCOOH)(bpyCH_2MV^{2+})(bpyCH_2PTZ)](PF_6)_4$ ($ZrO_2$−RuDA, solid line) in argon-deaerated acetonitrile at room temperature ($\lambda_{exc}$ = 455 nm; $\lambda_{mon}$ = 640 nm).

would be a lifetime component comparable to the model $[Ru(bpy)_2(bpyCOOH)]^{2+}$ adsorbed to $ZrO_2$, for which $\langle\tau\rangle$ = 223 ns ($\langle k\rangle = 4.5 \times 10^6$ $s^{-1}$).

This observation is consistent with the transient absorbance data shown in Figure 2. In solution, MLCT excitation of **1** is followed by oxidative quenching and $PTZ \rightarrow Ru^{III}$ electron transfer (eq 3), which are rapid (on the time scale of ~10 ns for the transient absorbance measurements).[20] Consequently, no bleach is observed in the transient absorption difference spectrum at 450 nm, because of the loss of $Ru^{II} \rightarrow$ bpyCOOH ground-state absorption, and quenching is concomitant with the appearance of the $MV^{+\bullet}$−$PTZ^{+\bullet}$ RS state. On the surface, a strong bleach appears at 450 nm, which decays with $\langle k_q\rangle = 2.5 \times 10^7$ $s^{-1}$, which is consistent with slower quenching of the initial MLCT state $ZrO_2$−$[Ru^{III}(bpy^{-\bullet}\ COOH)(bpyCH_2MV^{2+})(bpyCH_2PTZ)]^{4+}$. Decay of the bleach is concomitant with the appearance of the transient $MV^{+\bullet}$−$PTZ^{+\bullet}$ RS state.

Based on these results, intramolecular electron-transfer quenching of the initial MLCT excited state is inhibited in **1** when it is adsorbed to the mesoporous surface. This is the origin of the increase in surface emission quantum yield, compared to solution (see Table 1). Assuming that the unquenched MLCT lifetime is that of the surface-adsorbed model ($ZrO_2$−$[Ru(bpy)_2(bpyCOOH)]^{2+}$), electron-transfer quenching of the initial MLCT excited state in surface-adsorbed **1** is ~80% efficient.

The inhibition to excited-state electron transfer is not dependent on the external medium. Essentially equivalent results were obtained whether dry films were exposed to air or acetonitrile. The absence of a medium effect on excited-state dynamics has also been reported for the MLCT excited state(s) of $[Ru(bpy)_2(4,4'\text{-}(PO_2H_3)_2bpy)](PF_6)_2$ (bpy = 2,2′-bipyridine) adsorbed onto $ZrO_2$.[25] In that work, the absence of a significant solvent dependence was attributed to occupation of surface sites within the open porous structure of the surface that were relatively shielded from the solvent.

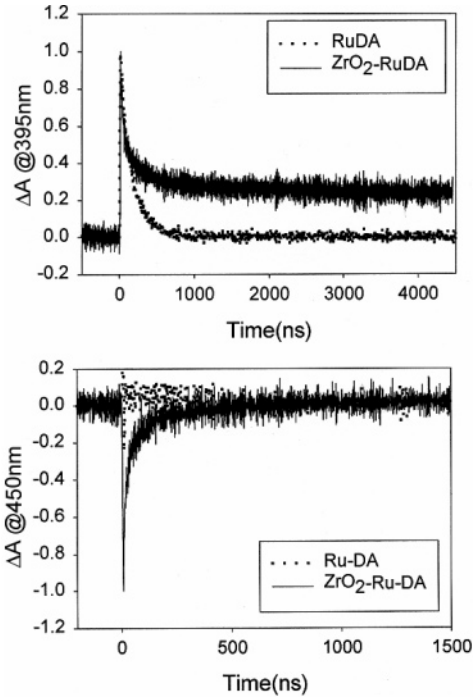


**Figure 2.** Comparison of transient absorbance ($\Delta A$) changes, versus time ($t$), for $[Ru(bpyCOOH)(bpyCH_2MV^{2+})(bpyCH_2PTZ)]^{4+}$ (RuDA, dotted line) and $ZrO_2$−$[Ru(bpyCOOH)(bpyCH_2MV^{2+})(bpyCH_2PTZ)](PF_6)_4$ ($ZrO_2$−RuDA, solid line) at (a) 395 nm and (b) 450 nm (bleach) in argon-deaerated acetonitrile at room temperature ($\lambda_{exc}$ = 455 nm).

The actual structure at the surface is unknown. A molecular modeling study on $[Ru(bpy)_2(bpyCO_2H)]^{2+}$ on glass suggested surface binding by surface ≡Si−OC(O)− ester formation to one carboxylate and hydrogen bonding to a second.[26] In addition, there are presumably $PF_6^-$ counterions on the surface for charge neutralization with the surface binding being best represented as $ZrO_2$−$[O_2CbpyRu(bpyCH_2MV^{2+})(bpyCH_2PTZ)](PF_6)_3$.

The inhibition to oxidative excited-state electron-transfer quenching by $MV^{2+}$ on the surface is puzzling and may be related to the fact that we were unable to observe the $MV^{2+/+}$ couple on the surface electrochemically. Oxidative quenching by appended $MV^{2+}$ in solution occurs with $\Delta G° = -0.3$ eV.[20] From the redox potential values in Table 1, the potentials for both the $Ru^{III/II}$ and $PTZ^{+/0}$ couples are increased by ~0.1 V on the surface. A similar increase in the $MV^{2+/+}$ potential on the surface would make the $\Delta G°$ value for $MV^{2+}$ quenching even more favorable, which suggests a kinetic origin for inhibited quenching by appended $MV^{2+}$.

In fact, the actual quenching mechanism on the surface is unknown and may involve initial reductive quenching by PTZ, followed by rapid bpy $\rightarrow MV^{2+}$ electron transfer. As long as the quenching step is rate limiting, either sequence would lead to the redox-separated state in eq 3.

**SCHEME 1**

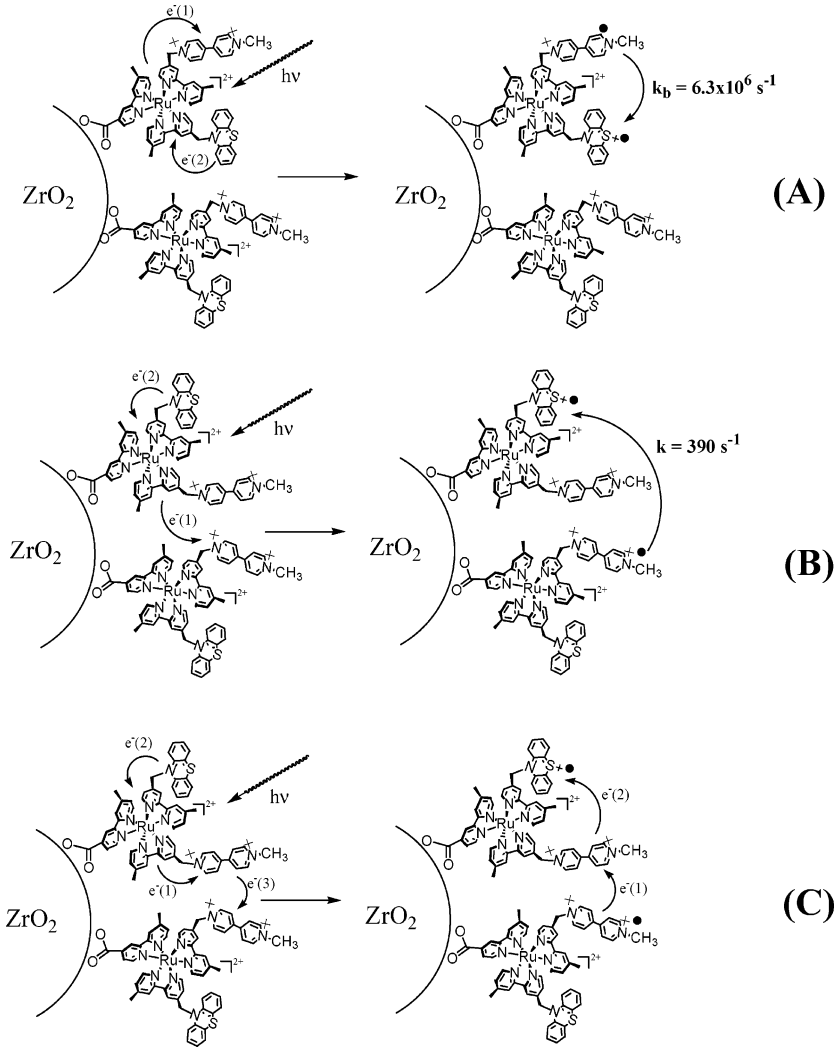


**Back-Electron Transfer.** Figure 2 compares transient absorbance kinetic traces for **1** in solution and adsorbed onto $ZrO_2$. The data illustrate the absorbance changes at wavelengths where $MV^{+\bullet}$ dominates (395 nm) and where the excited-state bleach dominates (450 nm).

At the earliest observation times, the spectral changes at these wavelengths are consistent with the growth of $MV^{+\bullet}$ and loss of the excited-state bleach, which is consistent with the quenching process in eq 3. As noted previously, the relatively slow disappearance of the bleach is consistent with the transient emission results and the decreased time scale for excited-state quenching on the surface.

The kinetic decay traces in Figure 2 clearly indicate that there are both fast and slow processes for $MV^{+\bullet} \rightarrow PTZ^{+\bullet}$ back-electron transfer. Both lead to the return to the ground state on the surface. The fast process is consistent with intramolecular electron transfer as in solution and is illustrated by process A in Scheme 1 for the case where oxidative quenching ($PTZ-Ru^{II*}-MV^{2+} \rightarrow PTZ-Ru^{III}-MV^{+\bullet}$) is followed by rapid $PTZ-Ru^{III}-MV^{+\bullet}$ electron transfer.

The detailed kinetics of back-electron transfer on the surface are predicted to be more complex than in solution, resulting in part from the heterogeneous nature of the surface and the sensitivity of the electron-transfer process to the local environment. There is an additional complication from contributions to intramolecular electron-transfer dynamics from eight separate isomers. As discussed elsewhere,[27] the basis for the isomerism is the relative dispositions of the substituents on the separate bpy ligands. For the bpy analogues of **1**—$[Ru(bpy)(bpyCH_2-MV^{2+})(bpyCH_2PTZ)]^{4+}$ (**2**)—four isomers (shown below) have been separated, which differ in the relative spatial dispositions of the $-PTZ$ and $-MV^{2+}$ groups.[27]

The solution back-electron-transfer rate constants for these isomers fall in the range of $4.5 \times 10^6 - 8.7 \times 10^6\ s^{-1}$ ($\tau = 115-220$ ns) with an average value of $6.3 \times 10^6\ s^{-1}$ observed for the mixture in acetonitrile.[27]

Addition of the carboxylic group to the third bpy ligand in **2** creates a total set of eight isomers—two sets of the four isomers mentioned previously, with each set differing with regard to the relative position of the carboxylic acid group.

The surface data were fit to the monoexponential function in eq 1. The extracted lifetime was $\tau = 160$ ns ($k = 6.3 \times 10^6\ s^{-1}$) in argon-deaerated acetonitrile at room temperature. Given the aforementioned isomer analysis, this value is an average that reflects the contribution from the eight isomers alluded to previously. The similarity in average rate constants between the solution and surface kinetic measurements is no doubt coincidental; however, it does demonstrate that after quenching has occurred, the dynamical properties of the assemblies toward electron transfer are retained on the surface.

As can be seen from the data in Figure 3, the long-lived transient absorption component exhibits a significant dependence on surface coverage. More specifically, as the surface coverage is decreased, the contribution of the long-lived component

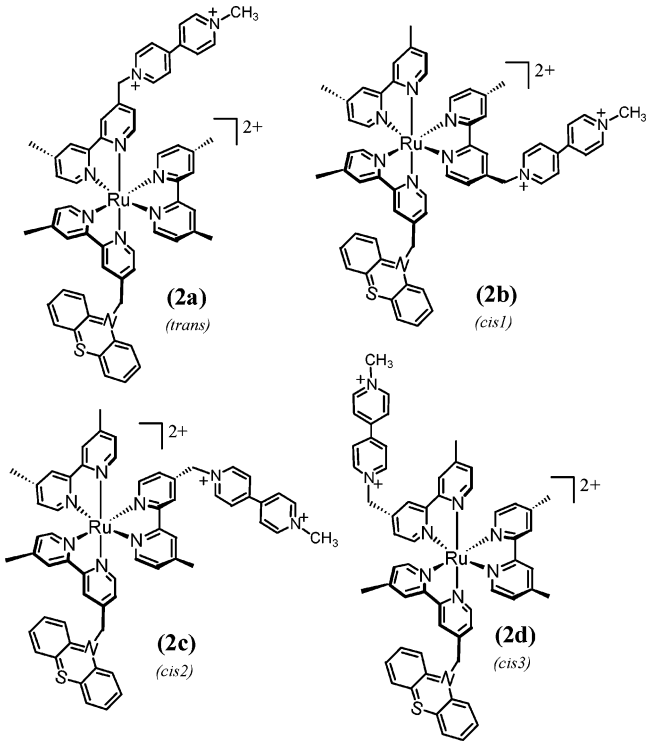


decreases and, as a result, the average rate constant for the decay of the observed transient increases.

The back-electron transfer for the slow component follows equal concentration, second-order kinetics. This is consistent with the decay of the long-lived transient component occurring by electron transfer between $PTZ^{+\bullet}$ and $MV^{+\bullet}$, which reside on different complexes that are spatially separated on the surface. Possible pathways for formation of the spatially isolated RS state are shown in processes B and C in Scheme 1. In process B of Scheme 1, the MLCT excited state is quenched directly by a $MV^{2+}$ group on an adjacent complex, followed by rapid intramolecular PTZ → $Ru^{III}$ electron transfer. An equivalent scheme could be written based on initial intermolecular quenching by PTZ. In process C of Scheme 1, initial intramolecular MLCT quenching by $MV^{2+}$ is followed by $MV^{+\bullet} \rightarrow MV^{2+}$ intermolecular electron transfer across the surface.

The net effect of any of these electron-transfer sequences is the formation of a spatially separated RS state involving neighboring molecules on the surface. Subsequent $PTZ \rightarrow PTZ^{+\bullet}$ or $MV^{+\bullet} \rightarrow MV^{2+}$ intermolecular electron-transfer hopping across the surface would have the effect of further isolating the stored $PTZ^{+\bullet}$ and $MV^{+\bullet}$ redox equivalents on the surface.

As noted previously, decay of the spatially separated RS state follows second-order, equal-concentration kinetics (eq 2), yielding $k = 390\ M^{-1}\ s^{-1}$ ($\tau = 2.6$ ms) for the fully loaded surface. From the isomer analysis, $k$ includes contributions from eight different RS isomers and a multitude of pathways for back-electron transfer. Two such pathways are illustrated in Scheme 1. One involves direct, long-range $MV^{+\bullet} \rightarrow PTZ^{+\bullet}$ intermolecular electron transfer and is shown in process B of Scheme 1. A second involves $MV^{+\bullet} \rightarrow MV^{2+}$ intermolecular electron transfer, followed by $MV^{+\bullet} \rightarrow PTZ^{+\bullet}$ intramolecular electron transfer (process C in Scheme 1).

Although the thermodynamic driving force for intermolecular and intramolecular electron transfer should be almost the same (presumably close to $\Delta G^\circ \approx -1.15$ eV for intramolecular electron transfer in solution[20]), there is a dramatic increase in time scale for the intermolecular process, because the redox sites

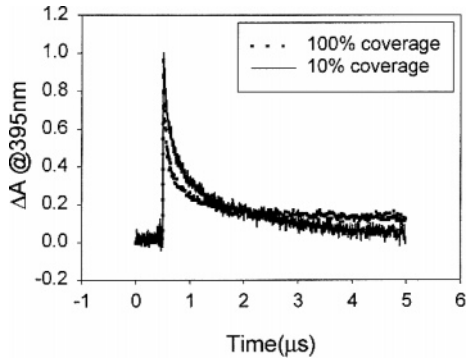


**Figure 3.** Comparison of $\Delta A$ vs $t$ changes for $ZrO_2$−[Ru(bpyCOOH)(bpyCH$_2$MV$^{2+}$)(bpyCH$_2$PTZ)](PF$_6$)$_4$ at 395 nm for 100% surface coverage (dotted line) and 10% surface coverage (solid line) in argon-deaerated acetonitrile at room temperature.

are spatially separated across the $ZrO_2$ surface. Earlier results on $ZrO_2$ have illustrated the importance of spatial separation between adsorbed $Ru^{II}$ and $Os^{II}$ polypyridyl complexes in determining rate constants for both ground-state electron transfer[28] and excited-state energy[25] transfer. Although not analyzed quantitatively, the results in Figure 3 illustrate the importance of the extent of surface loading both on the extent of formation of the long-lived transient and on the time scale for back-electron transfer.

The results presented are also of interest for the insight that they give into possible approaches to optical information storage and controlled time delays with the time-dependent optical properties of these materials being dependent on the composition of surfaces that have been modified by adsorbed molecular assemblies.

**Acknowledgment.** The authors acknowledge the support of the Department of Energy, under Grant No. DE-FG-02-96ER14607 (T.J.M.). We would like to also thank Dr. Kimberly Maxwell for providing samples of the [Ru(bpyCOOH)(bpyCH$_2$-MV$^{2+}$)(bpyCH$_2$PTZ)](PF$_6$)$_4$ salt.

## References and Notes

(1) Meyer, T. J. *Acc. Chem. Res.* **1989**, *22*, 163−170.
(2) Bard, A. J.; Fox, M. A. *Acc. Chem. Res.* **1995**, *28*, 141−145.
(3) Balzani, V., Ed. *Electron Transfer in Chemistry*; Wiley−VCH: Weinheim, New York, 2001.
(4) Kalyanasundaram, K.; Gratzel, M. *Coord. Chem. Rev.* **1998**, *177*, 347−414.
(5) Durr, H.; Bossmann, S. *Acc. Chem. Res.* **2001**, *34*, 905−917.
(6) Gao, F. G.; Bard, A. J. *Chem. Mater.* **2002**, *14*, 3465−3470.
(7) Maness, K. M.; Masui, H.; Wightman, R. M.; Murray, R. W. *J. Am. Chem. Soc.* **1997**, *119*, 3987−3993.
(8) Rudmann, H.; Shimada, S.; Rubner, M. F. *J. Am. Chem. Soc.* **2002**, *124*, 4918−4921.
(9) Wu, A. P.; Lee, J.; Rubner, M. F. *Thin Solid Films* **1998**, *329*, 663−667.
(10) Ishiji, T.; Kudo, K.; Kaneko, M. *Sens. Actuators B* **1994**, *22*, 205−210.
(11) Grant, S. A.; Satcher, J. H.; Bettencourt, K. *Sens. Actuators B* **2000**, *69*, 132−137.
(12) Chan, C. M.; Fung, C. S.; Wong, K. Y.; Lo, W. H. *Analyst* **1998**, *123*, 1843−1847.
(13) Mills, A.; Thomas, M. D. *Analyst* **1998**, *123*, 1135−1140.
(14) Martin, A. F.; Nieman, T. A. *Biosens. Bioelectron.* **1997**, *12*, 479−489.
(15) Carlson, B.; Phelan, G. D.; Kaminsky, W.; Dalton, L.; Jiang, X. Z.; Liu, S.; Jen, A. K. Y. *J. Am. Chem. Soc.* **2002**, *124*, 14162−14172.
(16) Xu, W. Y.; Kneas, K. A.; Demas, J. N.; DeGraff, B. A. *Anal. Chem.* **1996**, *68*, 2605−2609.
(17) Chen, P.; Meyer, T. J. *Chem. Rev.* **1998**, *98*, 1439−1477.
(18) Jones, W. E.; Chen, P.; Meyer, T. J. *J. Am. Chem. Soc.* **1992**, *114*, 387−388.
(19) Chen, P.; Meyer, T. J. *Inorg. Chem.* **1996**, *35*, 5520−5524.

(20) Maxwell, K. A.; Sykora, M.; DeSimone, J. M.; Meyer, T. J. *Inorg. Chem.* **2000**, *39*, 71−75.
(21) Sykora, M.; Maxwell, K. A.; DeSimone, J. M.; Meyer, T. J. *Proc. Natl. Acad. Sci. U.S.A.* **2000**, *97*, 7687−7691.
(22) Heimer, T. A.; Meyer, G. J. *J. Lumin.* **1996**, *70*, 468−478.
(23) Yonemoto, E. H.; Saupe, G. B.; Schmehl, R. H.; Hubig, S. M.; Riley, R. L.; Iverson, B. L.; Mallouk, T. E. *J. Am. Chem. Soc.* **1994**, *116*, 4786−4795.
(24) Yonemoto, E. H.; Riley, R. L.; Kim, Y. I.; Atherton, S. J.; Schmehl, R. H.; Mallouk, T. E. *J. Am. Chem. Soc.* **1992**, *114*, 8081−8087.
(25) Trammell, S. A.; Yang, P.; Sykora, M.; Fleming, C. N.; Odobel, F.; Meyer, T. J. *J. Phys. Chem. B* **2001**, *105*, 8895−8904.
(26) Meyer, T. J.; Meyer, G. J.; Pfennig, B. W.; Schoonover, J. R.; Timpson, C. J.; Wall, J. F.; Kobusch, C.; Chen, X. H.; Peek, B. M.; Wall, C. G.; Ou, W.; Erickson, B. W.; Bignozzi, C. A. *Inorg. Chem.* **1994**, *33*, 3952−3964.
(27) Treadway, J. A.; Chen, P.; Rutheford, T. J.; Keene, F. R.; Meyer, T. J. *J. Phys. Chem. A* **1997**, *101*, 6824−6826.
(28) Trammell, S. A.; Wimbish, J. C.; Odobel, F.; Gallagher, L. A.; Narula, P. M.; Meyer, T. J. *J. Am. Chem. Soc.* **1998**, *120*, 13248−13249.